Please provide feedback

Please support the ScholarWorks@UMBC repository by emailing scholarworks-group@umbc.edu and telling us what having access to this work means to you and why it's important to you. Thank you.

A planet within the debris disk around the pre-main sequence star AU Mic

Peter Plavchan[1*], Thomas Barclay[2], Jonathan Gagné[3], Peter Gao[4,5], Bryson Cale[1], William Matzko[1], Diana Dragomir[6,7], Sam Quinn[8], Dax Feliz[9], Keivan Stassun[9], Ian J.M. Crossfield[6,10], David A. Berardo[6], David W Latham[8], Ben Tieu[1], Guillem Anglada-Escudé[11], George Ricker[6], Roland Vanderspek[6], Sara Seager[6], Joshua N. Winn[12], Jon M. Jenkins[13], Stephen Rinehart[14], Akshata Krishnamurthy[6], Scott Dynes[6], John Doty[15], Fred Adams[16], Dennis A Afanasev[12], Chas Beichman[17,18], Mike Bottom[19], Brendan P. Bowler[20], Carolyn Brinkworth[21], Carolyn J. Brown[22], Andrew Cancino[23], David R. Ciardi[18], Mark Clampin[14], Jake T. Clark[22], Karen Collins[8], Cassy Davison[24], Daniel Foreman-Mackey[25], Elise Furlan[17], Eric Gaidos[26], Claire Geneser[27], Frank Giddens[23], Emily Gilbert[28], Ryan Hall[24], Coel Hellier[29], Todd Henry[30], Jonathan Horner[31], Andrew W. Howard[32], Chelsea Huang[6], Joseph Huber[23], Stephen R Kane[32], Matthew Kenworthy[33], John Kielkopf[34], David Kipping[35], Chris Klenke[23], Ethan Kruse[14], Natasha Latouf[1], Patrick Lowrance[36], Bertrand Mennesson[17], Matthew Mengel[22], Sean M. Mills[32], Tim Morton[37], Norio Narita[38,39,40,41,42], Elisabeth Newton[43], America Nishimoto[23], Jack Okumura[22], Enric Palle[42], Joshua Pepper[44], Elisa V. Quintana[14], Aki Roberge[14], Veronica Roccatagliata[45,46,47], Joshua E. Schlieder[14], Angelle Tanner[27], Johanna Teske[48], C. G. Tinney[49], Andrew Vanderburg[20,50], Kaspar von Braun[51], Bernie Walp[52], Jason Wang[31,4], Sharon Xuesong Wang[48], Denise Weigand[23], Russel White[24], Robert A. Wittenmyer[22], Duncan J. Wright[22], Allison Youngblood[14], Hui Zhang[53], Perri Zilberman[54]

[1]Department of Physics and Astronomy, George Mason University, 4400 University Drive, MSN 3F3, Fairfax, VA 22030, USA. [5]University of Maryland, College Park, Department of Astronomy, College Park, MD, 20742. [3]Institute for Research on Exoplanets, Université de Montréal, Département de Physique, C.P. 6128 Succ. Centreville, Montréal, QC H3C 3J7, Canada. [4]University of California, Berkeley, Berkeley, CA 94720, USA. [5]51 Pegasi b Fellow. [6]Massachusetts Institute of Technology, 54-1718 77 Mass. Avenue, Cambridge, MA, USA. [7]Department of Physics and Astronomy, University of New Mexico, Albuquerque, NM, USA. [8]Harvard-Smithsonian Center for Astrophysics, 60 Garden Street, Cambridge, MA 02138, USA. [9]Vanderbilt University, Department of Physics & Astronomy, 6301 Stevenson Center Lane, Nashville, TN 37235, USA. [10]Department of Physics & Astronomy, University of Kansas, 1251 Wescoe Hall Dr, Lawrence, KS 66045, USA. [11]School of Physics and Astronomy, Queen Mary, University of London, 327 Mile End Road, London, UK. [12]Department of Astrophysical Sciences, Princeton University, 4 Ivy Lane, Princeton NJ 08544, USA. [13]SETI Institute, 189 N Bernardo Ave suite 200, Mountain View, CA 94043, USA. [14]NASA Goddard Space Flight Center, Exoplanets and Stellar Astrophysics Laboratory, 8800 Greenbelt Road, Greenbelt, MD, 20771, USA. [15]Noqsi Aerospace Ltd, 15 Blanchard Ave., Billerica, MA, 01821, USA. [16]Department of Astronomy, University of Michigan, 108 S. University, 323 West Hall, Ann Arbor, Michigan, 48109-1107, USA. [17]Jet Propulsion Laboratory, California Institute of Technology, 4800 Oak Grove Drive, Pasadena, CA 91109-8099, USA. [18]NASA Exoplanet Science Institute, California Institute of Technology, M/C 100-22, 770 South Wilson Avenue, Pasadena, CA 91125, USA. [19]Institute for Astronomy, University of Hawaii at Manoa, 1680 East-West Road, Honolulu, HI 96822, USA. [20]The University of Texas at Austin, Astronomy 2515 Speedway, Stop C1400, Austin, TX 78712-1205, USA. [21]University Corporation for Atmospheric Research, 3090 Center

Green Drive, Boulder CO 80301, USA. [22]University of Southern Queensland, Centre for Astrophysics, Toowoomba, Qld 4350, Australia. [23]Missouri State University, Department of Physics, Astronomy and Materials Science, 901 S National Ave., Springfield, MO 65897, USA. [24]Department of Physics and Astronomy, Georgia State University, PO Box 4106, Atlanta, GA 30302-4106, USA. [25]Center for Computational Astrophysics, Flatiron Institute,162 5th Ave, New York, NY 10010, USA. [26]Department of Earth Sciences, University of Hawaii at Manoa, 1680 East-West Road, Honolulu, HI 96822, USA. [27]Mississippi State University, Department of Physics & Astronomy, Hilbun Hall, Starkville, MS, 39762, USA. [28]University of Chicago, The Department of Astronomy and Astrophysics, 5640 S. Ellis Avenue, Chicago, IL 60637, USA. [29]Keele University, Staffordshire, UK, ST5 5BG. [30]RECONS Institute, Chambersburg, PA 17201, USA. [31]Department of Astronomy, California Institute of Technology, 1200 E California Blvd, Pasadena, CA 91125, USA. [32]Department of Earth and Planetary Sciences, University of California, Riverside, CA 92521, USA. [33]Leiden Observatory, Leiden University, P.O. Box 9513, 2300 RA Leiden, The Netherlands. [34]Department of Physics and Astronomy, University of Louisville, Louisville, KY 40292, USA. [35]Department of Astronomy, Columbia University, 550 W 120th Street, New York, NY 10027, USA. [36]IPAC, California Institute of Technology, 1200 E California Blvd, Pasadena, 91125, USA. [37]Astronomy Department, University of Florida, 211 Bryant Space Science Center, P.O. Box 112055, Gainesville, FL 32611-2055, USA. [38]Department of Astronomy, The University of Tokyo, 7-3-1 Hongo, Bunkyo-ku, Tokyo 113-0033, Japan. [39]JST, PRESTO, 7-3-1 Hongo, Bunkyo-ku, Tokyo 113-0033, Japan. [40]Astrobiology Center, NINS, 2-21-1 Osawa, Mitaka, Tokyo 181-8588, Japan. [41]National Astronomical Observatory of Japan, NINS, 2-21-1 Osawa, Mitaka, Tokyo 181-8588, Japan. [42]Instituto de Astrofisica de Canarias (IAC), 38205 La Laguna, Tenerife, Spain. [43]Department of Physics & Astronomy, Dartmouth College, Hanover, NH 03755, USA. [44]Department of Physics, Lehigh University, 16 Memorial Drive East, Bethlehem, PA 18015, USA. [45]Dipartimento di Fisica "Enrico Fermi", Universita' di Pisa, Largo Pontecorvo 3, 56127 Pisa, Italy. [46]INAF-Osservatorio Astrofisico di Arcetri, Largo E. Fermi 5, 50125 Firenze, Italy. [47]INFN, Sezione di Pisa, Largo Pontecorvo 3, 56127 Pisa, Italy. [48]Observatories of the Carnegie Institution for Science, 813 Santa Barbara Street, Pasadena, CA 91101, USA. [49]Exoplanetary Science at UNSW, School of Physics, UNSW Sydney, NSW, 2052, Australia. [50]NASA Sagan Postdoctoral Fellow. [51]Lowell Observatory, 1400 W Mars Hill Road, Flagstaff, AZ 86001, USA. [52]NASA Infrared Telescope Facility, 640 North A'ohoku Place, Hilo, HI, 96720, USA. [53]School of Astronomy and Space Science, Key Laboratory of Ministry of Education, Nanjing University, Nanjing, China. [54]SUNY Stony Brook, 100 Nicolls Road, Stony Brook, NY 11794. *pplavcha@gmu.edu

AU Microscopii (AU Mic) is the second closest (d = 9.79 parsec) pre-main sequence (22 Myr[1]) star. AU Mic possesses a relatively rare[2] and spatially resolved[3] edge-on debris disk extending from ~35–210 astronomical units from the star[4], and with clumps exhibiting non-Keplerian motion[5-7]. Detection of newly-formed planets around such a star is challenged by the presence of spots, plage, flares and other manifestations of magnetic "activity" on the star[8-9]. Here we report observations of a planet transiting AU Mic. The transiting planet, AU Mic b, has an orbital period of 8.47 days, an orbital distance of 0.06 astronomical units, a radius of 0.4 Jupiter radii, and a mass less than 0.18 Jupiter masses at 3-σ confidence. This very young, nearby planet represents an

unparalleled opportunity to study its atmosphere and its interaction with the host star at a very early stage in its evolution.

NASA's Transiting Exoplanet Survey Satellite *(TESS)* mission[10] was launched on April 18, 2018, and monitored the brightness of AU Mic during the first 27 days of its survey of most of the sky. Two transits of AU Mic b appear in the *TESS* photometric light curve. Follow-up observations with the *Spitzer* Space Telescope[11] confirm the transits of AU Mic b. An additional, shallower candidate transit is observed in the *TESS* light curve, which suggests the possible existence of additional planets. Joint RV and high-resolution adaptive optics imaging rules out other planets in this system more massive than 1 $M_{Jupiter}$ interior to ~20 au[12]. The 3-σ upper limit to the velocity reflex motion semi-amplitude K for AU Mic b is K<28 m/s (see Methods), corresponding to an upper-limit for the mass of AU Mic b of < 0.18 $M_{Jupiter}$ or <3.4 $M_{Neptune}$.

The proximity, brightness, age, and edge-on geometry of the AU Mic system will permit us to study AU Mic b at an early stage of its dynamical, thermal, and atmospheric evolution, as well as any connection between the planet and residual debris disk. The host star is a red dwarf, one of the most abundant stellar types in our Galaxy. Their diminutive size, mass, and luminosity make middle-aged, comparatively inactive M dwarfs favored targets to search for Earth-size planets in circumstellar habitable zones. Thus AU Mic is an opportunity to study a possible antecedent to these important systems. Moreover, AU Mic, unlike most M dwarfs of a similar age, possesses a debris disk[2], and hence may offer insight into connections between planets and dust disks. This system confirms that gaseous planet formation and any primordial disk migration takes place in less than 20 Myr[13]. The accretion and migration of this (or additional) planets could have left behind the Kuiper-belt-like "birth ring" of parent body debris that is hypothesized at ~35 au[6], while clearing the interior disk of gas and dust. Furthermore, it is possible that any remnant primordial debris in the inner disk near the current locations of the planet could be in the process of being ejected by this planet (e.g. clearing out). Measurement of the spin-orbit obliquity of AU Mic b via the Rossiter-McLaughlin effect (~40 m/s peak-to-peak amplitude expected) or Doppler tomography would be an important test of migration models since we expect any obliquity in this young system to be unaffected by stellar tides and primordial.

AU Mic is a member of the the β Pictoris Moving Group; the group's archetype β Pic is a much more massive (~3.5x), luminous (~100x) and hotter (~2x) A-type star, also possessing a debris disk. β Pic has a more massive Jovian planet β Pic b observed by direct imaging at a semi-major axis of ~9 au, with a mass of ~11+/-2 $M_{Jupiter}$ determined with astrometry[14]. AU Mic and β Pic are of the same stellar age, but are very different exoplanet host stars. While AU Mic b possibly formed at a distance similar to β Pic b and then migrated inwards to its present location, β Pic b has not migrated inward significantly. These two coeval systems provide an excellent differential comparison for planet formation.

Finally, the combined effect of stellar winds and interior planets have been invoked to explain the high-speed ejection of dust clumps from the system[6-7]. The observed clumps are dynamically decoupled from AU Mic b; the ratio of the semi-major axes (0.06 au vs >35 au) is a

factor of >100, however the clumps could have originated much closer to the star. Dust produced in the debris ring at ~35 AU will spiral inwards primarily as a result of stellar wind drag, which, for AU Mic and a ~1000 times solar wind mass loss rate[6], is estimated to be 3700 times stronger than Poynting-Robertson drag[2]. To compare the time-scales between collisions of dusty debris and the stellar wind drag force[15] we assume a birth ring fractional width of 10% (3.5 au), and given AU Mic's infrared flux excess, find that the stellar wind drag and dust collision time-scales are roughly equal. Thus, some fraction of the dust grains generated in the birth ring at ~35 au may spiral inward to the host star under the action of stellar wind drag, instead of being ground down further by dust collisions until blown out of the system by radiation pressure. For 1 μm-sized solid grains of dusty debris, the inspiral time would take ~7500 years, much shorter than the age of the star. Such dust may have been observed by ALMA interior to the birth ring at ~35 au at <3 au[16]. Dust reaching the orbit of an interior planet could be dynamically ejected, depending on the Safronov number: we estimate that of "b" to be 0.07 and thus inefficient at ejecting dust.

There is no other known system that possesses all of these crucial pieces -- an M-dwarf star that is young, nearby, still surrounded by a debris disk within which are moving clumps and orbited by a planet with a direct radius measurement. As such, AU Mic provides a unique laboratory to study and model planet and planetary atmosphere formation and evolution processes in detail.

References

1 Mamajek, E.E.; Bell, Cameron P.M.; "On the age of the β Pictoris moving group." Mon. Not. R. Astron. Soc. 445, 3 (2014)
2 Plavchan, P; Jura, M.; & Lipscy, S.J.; "Where Are the M Dwarf Disks Older Than 10 Million Years?" Astrophys. J., 631, 2 (2005)
3 Kalas, P.; Liu, M.C.; Matthews, B.C.; "Discovery of a Large Dust Disk Around the Nearby Star AU Microscopii." Science, 303, 5666 (2004)
4 Strubbe, L.E.; & Chiang, E.I.; "Dust Dynamics, Surface Brightness Profiles, and Thermal Spectra of Debris Disks: The Case of AU Microscopii." Astrophys. J., 648, 1 (2006)
5 Boccaletti, A; et al.; "Fast-moving features in the debris disk around AU Microscopii." Nature, 526, 230 (2015)
6 Chiang, E.I.; & Fung, Jeffrey; "Stellar Winds and Dust Avalanches in the AU Mic Debris Disk." Astrophys. J., 848, 1, 4, (2017)
7 Sezestre, É; et al.; "Expelled grains from an unseen parent body around AU Microscopii." Astronomy & Astrophysics, 607, A65 (2017)
8 van Eyken, J.; et al.; "The PTF Orion Project: A Possible Planet Transiting a T-Tauri Star." Astrophys. J., 755, 1, 42 (2012).
9 Donati, J.F.; et al.; "A hot Jupiter orbiting a 2-million-year-old solar-mass T Tauri star." Nature, 534, 7609 (2016)
10 Ricker, G.R.; et al.; "Transiting Exoplanet Survey Satellite (TESS)." Journal of Astronomical Telescopes, Instruments, and Systems, 1, 014003 (2015)

11 Deming, D.; et al.; "Spitzer Secondary Eclipses of the Dense, Modestly-irradiated, Giant Exoplanet HAT-P-20b Using Pixel-level Decorrelation." The Astrophys. J., 805, 2, 132 (2015).

12 Lannier, J.; Lagrange, A. M.; Bonavita, M.; Borgniet, S.; Delorme, P.; Meunier, N.; Desidera, S.; Messina, S.; Chauvin, G.; Keppler, M.; "Combining direct imaging and radial velocity data towards a full exploration of the giant planet population. I. Method and first results." Astronomy & Astrophysics, 603, A54 (2017)

13 Kley, W.; Nelson, R. P.; "Planet-Disk Interaction and Orbital Evolution." Annual Review of Astronomy & Astrophysics, 50, 211-249 (2012)

14 Snellen, I. A. G.; Brown, A. G. A.; "The mass of the young planet Beta Pictoris b through the astrometric motion of its host star." Nature Astronomy, 2, 883-886 (2018)

15 Plavchan, P., et al; "New Debris Disks Around Young, Low-Mass Stars Discovered with the Spitzer Space Telescope." Astrophys. J., 698, 2, 1068-1094 (2009)

16 MacGregor, Meredith A.;et al.; "Millimeter Emission Structure in the First ALMA Image of the AU Mic Debris Disk." Astrophys.l J. Letters, 762, 2, L21 (2013)20 Cale, B.; et al.; "Precise Radial Velocities of Cool Low Mass Stars With iSHELL." Astrophys. J., in press (2019)

17 Chen, JingJing, & Kipping, D.; "Probabilistic Forecasting of the Masses and Radii of Other Worlds." The Astrophys. J., 834, 1, 17, (2017)

18 White, Russel; et al.; "Stellar Radius Measurements of the Young Debris Disk Host AU Mic." American Astronomical Society, AAS Meeting #233, id. 259.41

19 Torres, C.A.O.; Ferraz Mello, S.; & Quast, G.R.; "HD 197481: A Periodic dMe Variable Star." Astrophys. J. Letters, 11, 13-14 (1972)

Figures and Tables
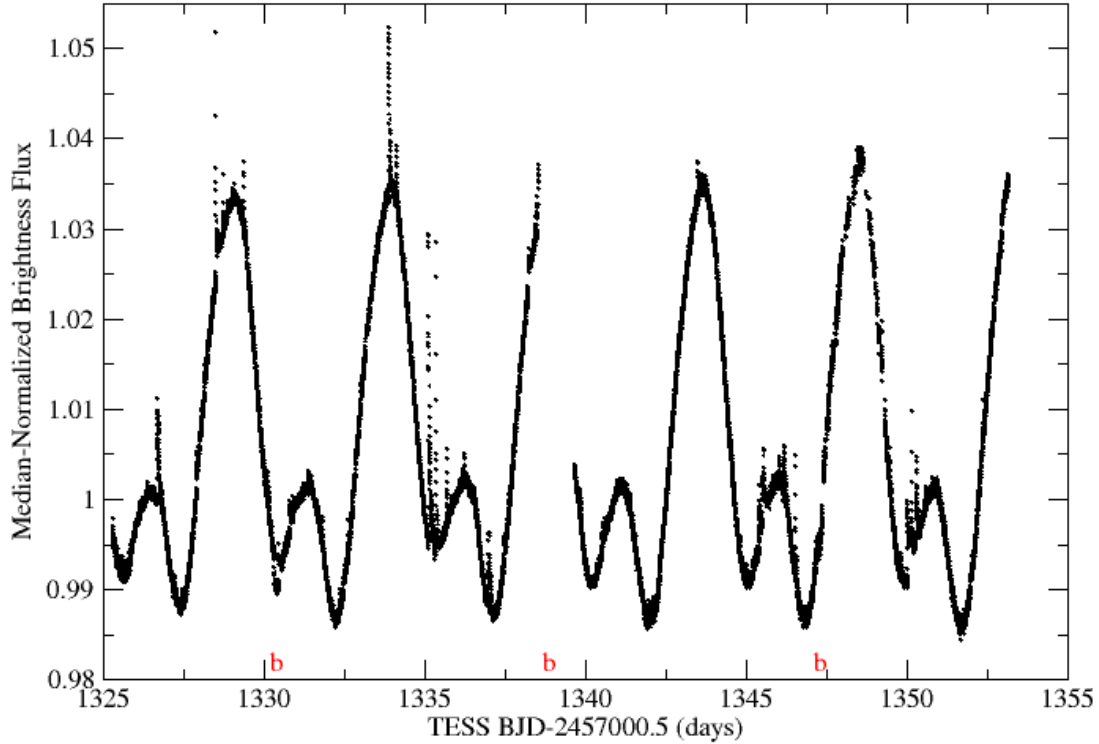
Figure 1 TESS light curve for AU Mic. Black dots are plotted as normalized flux as a function of time, obtained from MAST archive. Transit ephemerides of AU Mic b are indicated in red. The double-humped sinusoidal-like pattern is due to the rotational modulation of starspots, with the 4.863d rotation period readily apparent. The large, brief vertical streaks of data points deviating upwards from this slower modulation are due to flares. Data with non-zero quality flags indicating the presence of spacecraft-related artifacts, such as momentum dumps, are removed. The gap at ~1339 days corresponds to the data downlink with Earth during the spacecraft's perigee. A third transit of AU Mic b was missed during this data downlink data gap, and thus the orbital period of AU Mic b is one-half of period inferred from the two TESS transit events seen. AU Mic exhibited flaring activity with energies ranging from $10^{31.6}$ to $10^{33.7}$ ergs in the TESS bandpass over the 27 day light curve (+/- ~60%), with a mean flare amplitude of 0.01 relative flux units. 1-σ measurement uncertainties are smaller than the symbols shown (<1 ppt).
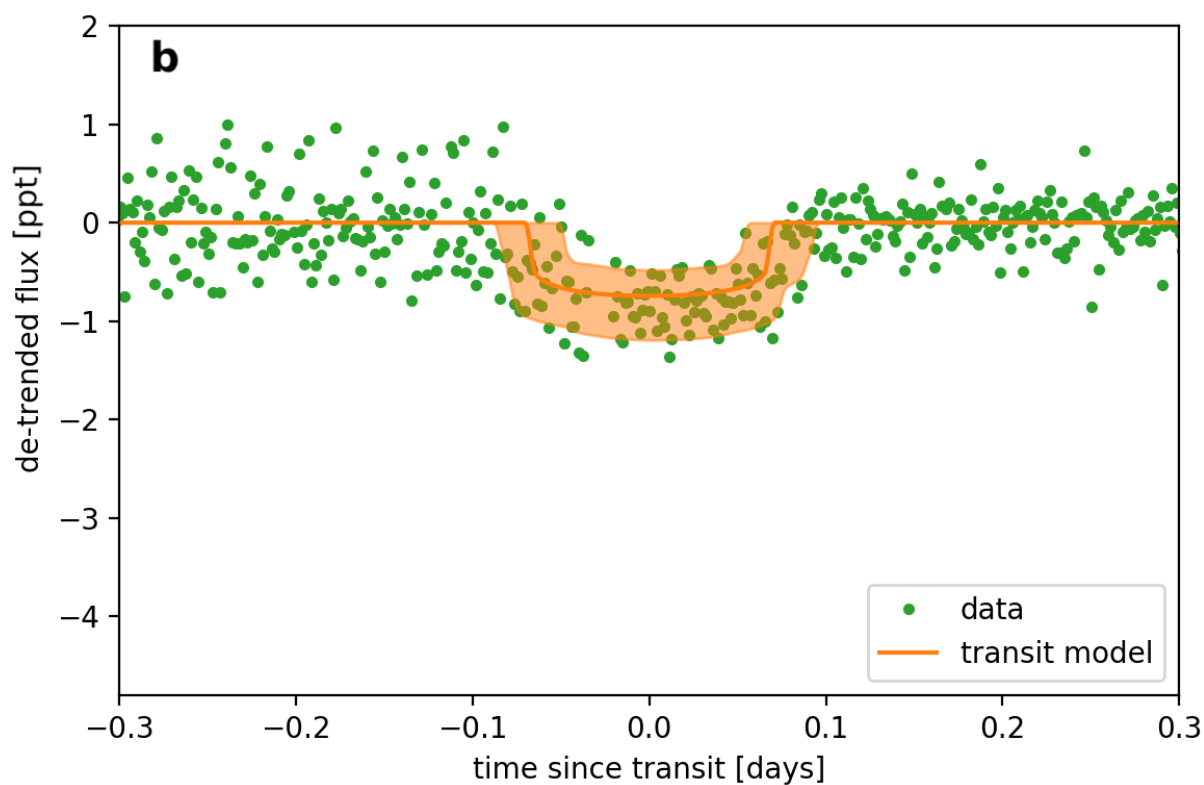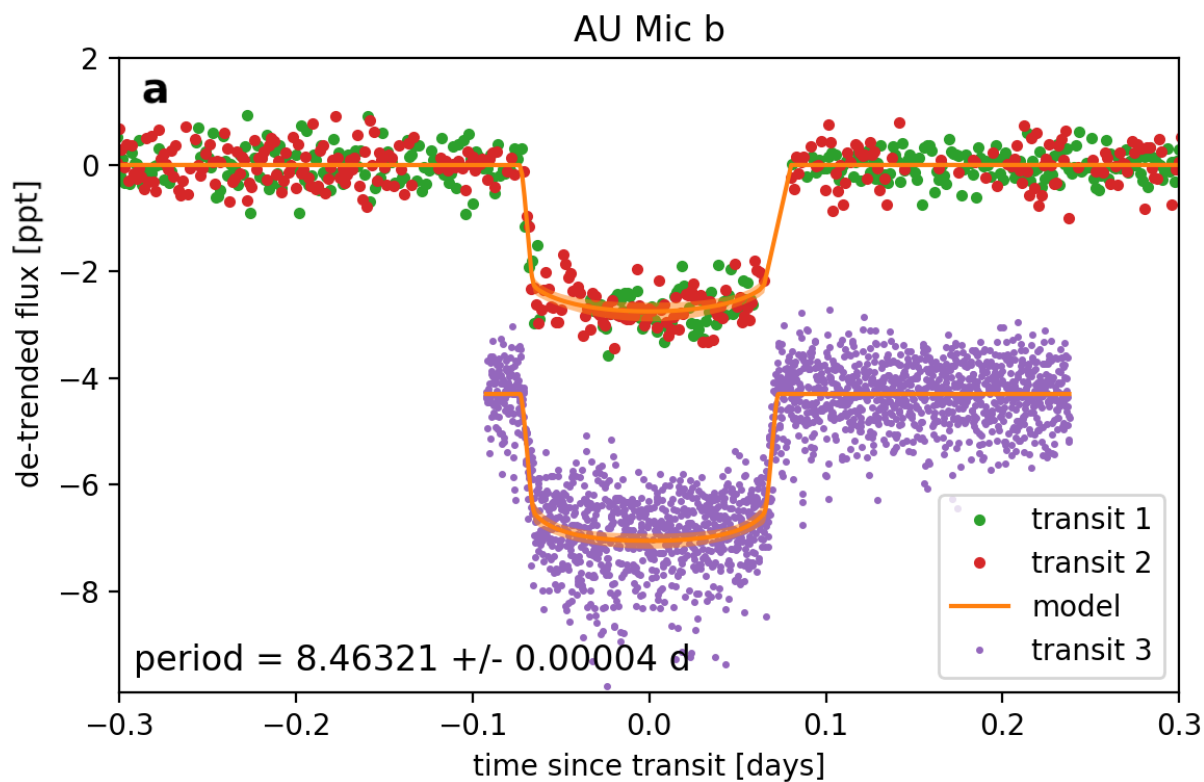
Figure 2: TESS visible light (blue and green circles) and Spitzer IRAC[11] 4.5 μm (purple circles)

light curves of the transits of AU Mic b and a separate, single candidate transit event. **a** The data for transits of AU Mic b are shown with an arbitrary vertical shift applied for clarity; flux units are parts per thousand, or ppt. The transit model (orange curve) includes a photometric model that accounts for the stellar activity modeled with a Gaussian Process, which is subtracted from the data before plotting. The frequent flares from the stellar surface are removed with an iterative sigma-clipping (see Methods). In particular, flares are observed during the egress of the both TESS transits of AU Mic b, and also just after the ingress of the second transit of AU Mic b. The presence of these flares in the light curve particularly impact our precision in measuring the transit duration and thus the mass/density of the host star AU Mic and consequently the impact parameter and eccentricity of the orbit of AU Mic b. Model uncertainties shown as shaded regions are 1-σ c.i.. The uncertainty in the out-of-transit baseline is ~0.5 ppt but not shown for clarity. **b** The AU Mic candidate single transit signal, identified by visual inspection of the *TESS* light curve. The change in noise before and after the candidate transit signal is due to a "dump" of angular momentum from the spacecraft reaction wheels which decreased the pointing jitter and improved the photometric precision; data points during the dump are not shown.
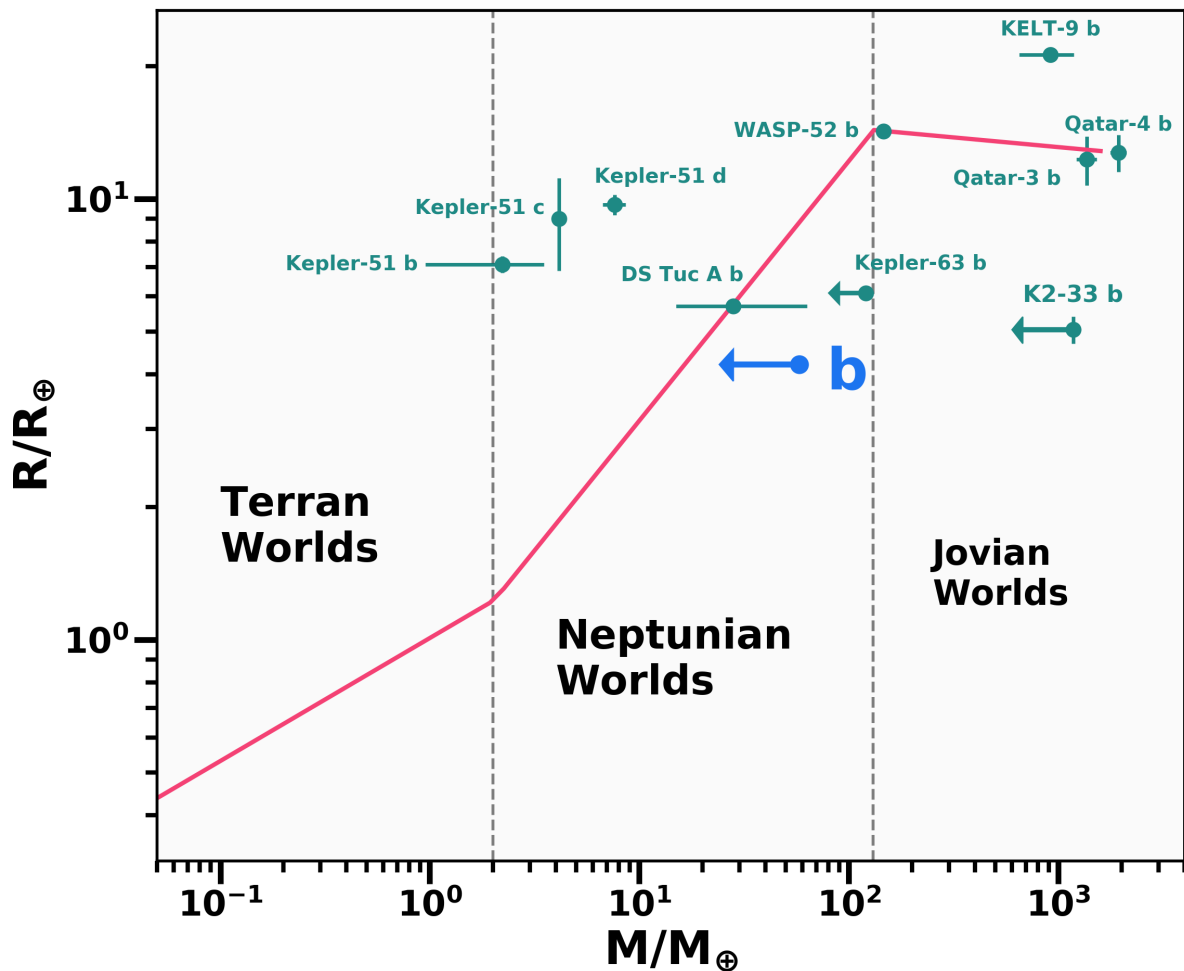
Figure 3: Mass-radius diagram for AU Mic b in the context of "mature" exoplanets and known young exoplanets. AU Mic b is shown in blue. We compare it to the nominal best-fit mass-radius relationship from known exoplanets orbiting older main sequence stars[17] shown as a red segmented line (dispersion not shown), and known exoplanets from the NASA Exoplanet Archive with measured masses or mass upper limits, radii, and estimated stellar host ages <=400 Myr: DS Tuc A b (mass is estimated from Ref 17 and not measured), Kepler-51 bcd, 63 b, K2-33 b, Qatar-3 b,4 b, KELT-9 and WASP-52 b. By combining the radius measurement from *TESS*, and the mass upper limit from RVs, we can ascertain an upper limit to the planet density for AU Mic b to critically inform models for planet formation. Our current upper limit for the mass of AU Mic b cannot rule out a density consistent with Neptune-like planets orbiting older main sequence stars, but a more precise constraint or measurement in the future may show it to be inflated. Uncertainties shown are 1-σ for detections, and 3-σ for mass upper-limits.

Table 1. System parameters table

Parameter	68% Credible Interval	Remarks
AU Mic (star)		
Distance from the Sun	9.79+/-0.04 parsecs	Gaia mission parallax
Radius	0.75+/- 0.03 R_{sol}	Directly measured with interferometry[18]
Mass	0.50 +/-0.03 M_{sol}	Estimated from spectral type and age, and consistent with independently fitting the two transit events in TESS light curve for AU Mic b
T_{eff}	3700 +/- 100 K	Spectral Energy Distribution modeling[15]
Luminosity	0.09 L_{sol}	Spectral Energy Distribution modeling[15]
Age	22+/-3 Myr	[1]
Rotation period	4.863+/-0.010 days	RV analysis, TESS light curve, SuperWASP light curve[19]
Projected rotational velocity	8.7+/-0.2 km/s	[12]
Linear Limb-Darkening Coefficient (TESS)	0.21+0.20-0.15	TESS light curve
Quadratic Limb-Darkening Coefficient (TESS)	0.0+0.18-0.14	TESS light curve

Linear Limb-Darkening Coefficient (Spitzer)	0.17+0.22-0.12	Spitzer light curve
Quadratic Limb-Darkening Coefficient (Spitzer)	0.15+0.27-0.21	Spitzer light curve
Visible stellar activity amplitude	145+17-14 m/s	RV analysis
Near-Infrared stellar activity amplitude	80+16-12 m/s	RV analysis; K-band at 2.3 μm
Spot decay half-life	110+/-30 days	RV analysis
Gaussian Process hyper-parameter 4	0.37+/-0.02	RV analysis
Apparent Magnitudes	TESS = 6.76 mag V = 8.81 mag I = 6.59 mag J = 5.44 mag K = 4.53 mag	
AU Mic b		
Period	8.46321+/-0.00004 days	TESS & Spitzer transit light curve analysis
Semi-major axis	0.066+0.007-0.006 au	TESS & Spitzer transit light curve analysis
Velocity Semi-Amplitude K	<28 m/s	RV analysis
Mass	< 3.4 $M_{Neptune}$ < 0.18 $M_{Jupiter}$	RV analysis
Radius	1.08+/- 0.05 $R_{Neptune}$ 0.375 +/-0.018 $R_{Jupiter}$	TESS & Spitzer transit light curve
Density	<4.4 g/cm^3	RV / TESS analysis
Time(s) of Conjunction (Barycentric Julian Day)	2458330.39153+0.00070-0.00068 days	TESS & Spitzer transit light curves
Transit Duration (τ_{14})	3.50+0.63-0.59 hr	TESS & Spitzer transit light curves
R_p/R_*	0.0514+/-0.0013	TESS & Spitzer transit light curve
Impact parameter b	0.16+0.14-0.11	TESS & Spitzer transit light curve

a/R$_*$	19.1+1.8/-1.6	TESS & Spitzer transit light curve
eccentricity	0.10+0.17-0.09	TESS & Spitzer transit light curve; circular orbit assumed for RV analysis
Candidate transit event		
Period	30+/-6 days	TESS light curve transit duration
Radius	0.60+/-0.17 R$_{Neptune}$ = 0.21 +/-0.06 R$_{Jupiter}$	TESS transit light curve
Time(s) of Conjunction	2458342.22+/-0.03 days	TESS transit light curve
R$_p$/R$_*$	0.028 +/-0.006	TESS transit light curve
Impact parameter b	0.5+/-0.3	TESS transit light curve
a/R$_*$	40+/-8	TESS transit light curve
Eccentricity	0.2+/-0.2	TESS transit light curve

Methods:

TESS light curve analysis

AU Mic has long been known as a young star exhibiting flares and brightness variations driven by large starspots on the stellar surface rotating in and out of view[20]. Previous attempts to find transiting planets were not successful due to this variability and the redness of the star combined with secondary atmospheric extinction effects[21-22], in spite of reasoning that the orbits of any planets could be aligned with AU Mic's edge-on debris disk, and therefore could be more likely to transit than for a random inclination.

TESS observed AU Mic (TIC 441420236) in its first sector (2018 July 25 -- August 22). The _TESS_ light curve from the 2-minute cadence stamp was processed by the Science Processing Operations Center pipeline, a descendant of the _Kepler_ mission pipeline based at the NASA Ames Research Center[23-24]. After visually identifying the transits in the light curve, we independently validate the existence of the transits from the 30 minute full-frame image (FFI) data. We also extract light curves with different photometric apertures, and confirm the transit signal is robust and consistent. No centroid motion is observed during transits, suggesting that it is associated with AU Mic rather than an instrumental systematic or contamination from scattered background light or a distant star. To validate the transit with ancillary data, we inspect archival sky survey images such as POSS and find no background stars within the TESS pixels

that are present at the location of AU Mic with a sufficient brightness ratio so as to mimic the observed transit signals with a background eclipsing binary. Nor do we or others identify any background eclipsing binaries in high-contrast adaptive optics imaging[3] nor our high-resolution spectroscopy (see below). The nearest Gaia DR2 source that is capable of producing a false positive if an eclipsing binary (Gmag contrast = 5.7 mag, ignoring TESS-G-band color terms) is 76 arcsec or 3 TESS pixels from AU Mic. Finally, the interferometric stellar radius determination[18] rules out bound stellar companions.

We perform multiple independent analyses of the TESS light curve to identify and model the transits present, including the TESS mission pipeline planet detection algorithms, ExoFAST v1.0 and v2.0[25-26], and astrodensity profiling[27] which yield consistent results. While ExoFAST does support the simultaneous modeling of light curves and RVs, it does not include components for modeling the stellar activity prevalent for AU Mic in the RVs. Thus, we carry out independent analyses of the light curves and RVs. For the light curves, ExoFAST and astrodensity profiling do not simultaneously model the exoplanet transits and detrending of the photometric variability produced by the rotational modulation of the starspots. Thus to prepare the TESS light curves for these analysis tools, we first fit four sinusoids to the light curve with periods equal to the rotation period, and one-half, one-third, and one-quarter thereof. We then apply a 401 data-point running median filter to remove the remaining photometric modulation due to starspots. The flares present in the transit events were not removed for these analyses, primarily impacting the determination of the transit duration of AU Mic b.
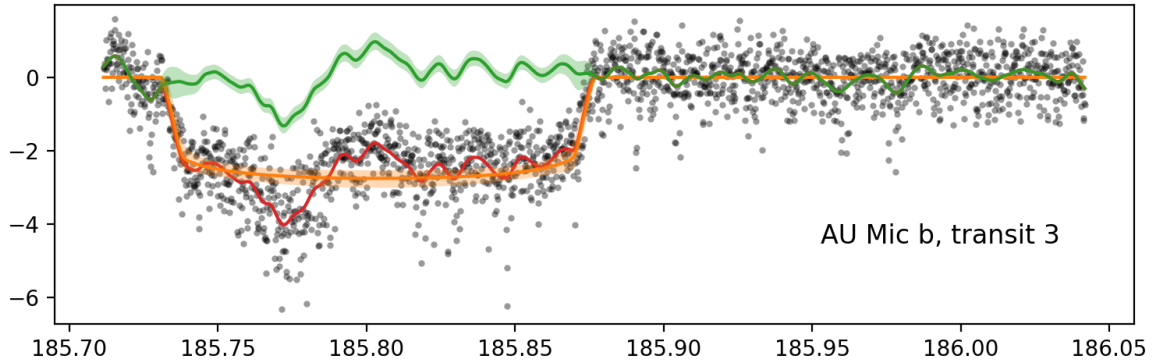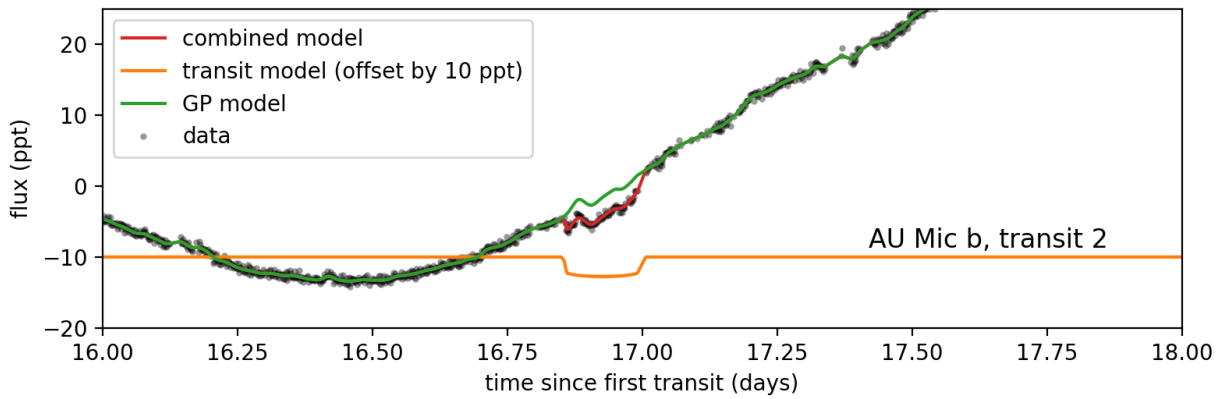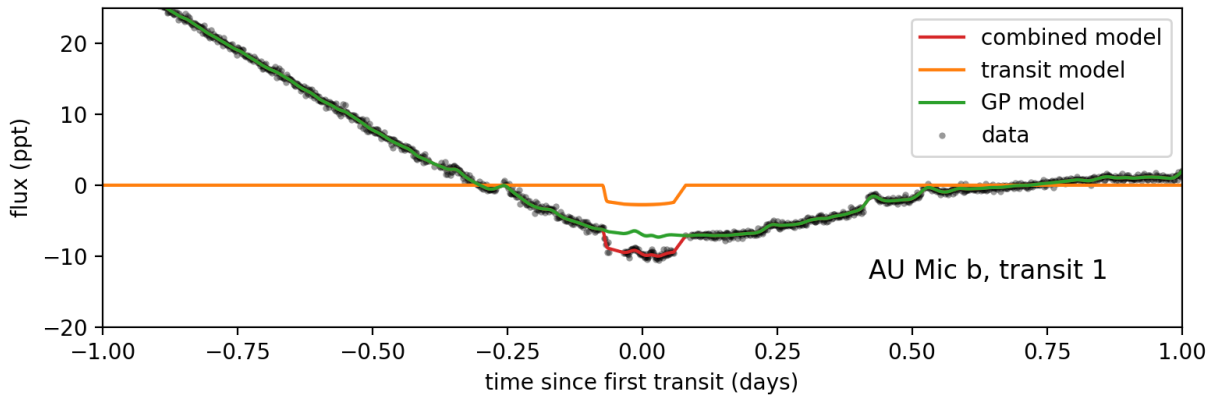
Spitzer light curve analysis

Due to the data collection gap in the TESS light curve, Spitzer Director's Discretionary Time (DDT; PID #14214. 17.3 hr) observations were proposed, awarded and collected in 2019 to rule in or rule out one-half of the orbit period for AU Mic b as seen in the TESS light curve. Two transits were observed with IRAC at 4.5 μm, one of which is presented herein, and the latter will be presented in a future paper. We first clean up the raw images: sigma-clipping outliers, and subtracting off a background estimate from an annulus around the center of light. We then sum the flux in a circular aperture centered around the center of light of each frame, and do this for several different aperture radii. We then follow the procedure from Ref 11 and do a Pixel Level Decorrelation (PLD; using 3x3 pixels) on each radius, and pick the one that gives the smallest scatter. We adopt a 2.4 pixel radius aperture, binned by a factor of 106.

Joint TESS and Spitzer photometric analysis

We carry out a custom analysis that simultaneously accounts for the rotational modulation of starspots, the flares and the transit events for both the TESS and Sptizer light curves to evaluate the impact our detrending of the spot rotational modulation and flares have on our analysis of the transit events, and this is the analysis we adopt in the main paper. We use the TESS pre-search data conditioned light curve created by the TESS pipeline[24,28,29] for this analysis. To remove flares, we create a smoothed version for the light curve by applying a third order Savitzy-Golay filter with a window of 301 data points, subtracting the smooth light curve,

and clipping out data points more deviant than 1.5x the rms. We performed 10 iterations of this clipping, removing the majority of stellar flares. We then used the exoplanet package (https://github.com/dfm/exoplanet) to simultaneously model the stellar variability and transits. Exoplanet uses several other software packages: Starry for the transit model (https://github.com/rodluger/starry), and celerite (https://github.com/dfm/celerite) for the GP, which we use to model stellar variability. Our GP model consists of two terms, a term to capture long term trends, and a term to capture the periodic modulation of the stars light curve that is caused by spots on the stellar surface. The latter is a mixture of two stochastically-driven, damped harmonic oscillator terms that can be used to model stellar rotation. It has two modes in Fourier space: one at the rotation period of the star and one at half the rotation period. The transit model is parameterized by two stellar limb darkening parameters[55], the log of the orbital period, log stellar density, the time of first transit, log of the planet-to-star radius ratio, the impact parameter of the transit, orbital eccentricity of the planet, and the periastron angle.

We next run an mcmc to fit for the 9 PLD coefficients (the c_i's), a slope + quadratic ramp to represent the rotational modulation of the stellar activity still visible for AU Mic in the Spitzer light curve at 4.5 μm, as well as a transit model including two limb darkening coefficients for a quadratic limb darkening law. We leave the photometric uncertainty to be a free parameter, which we fit for during the mcmc Prior to the mcmc, we cut out the dip that occurs during the transit, potentially due to a large spot crossing, from BMJD = 58524.5 to 58524.53, to make sure we weren't biasing the transit depth. The systematics-corrected light curve is used in our light curve modeling in the main text.
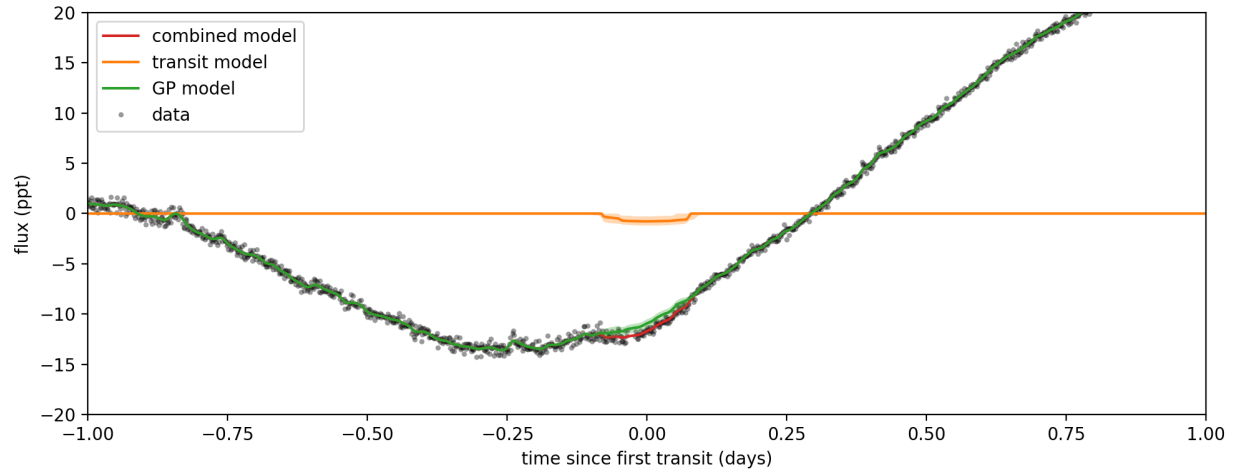
Extended Data Figure 1 The TESS and Spitzer light curves for AU Mic centered on four transit events. **a** and **b** Two TESS transits for AU Mic b, with the model components plotted as indicated in the legend. A flare is present during the egress of the first transit of AU Mic b, and a flare is present just after the ingress during the second transit of AU Mic b. While unfortunate timing, flares of this amplitude are pervasive throughout the TESS light curve for AU Mic, and complicate the recovery of these events from automated transit search algorithms. **c** The Spitzer transit observation of AU Mic b. The deviations in transit are not instrumental and the subject of a future paper, and are likely related to the planet crossing large active regions on the stellar surface. **d** The ~1 ppt candidate single transit event seen in the TESS light curve. For all panels, 1-σ measurement uncertainties are suppressed for visual clarity and are <1 ppt. 1-σ model uncertainties in transit are shown as shaded regions.
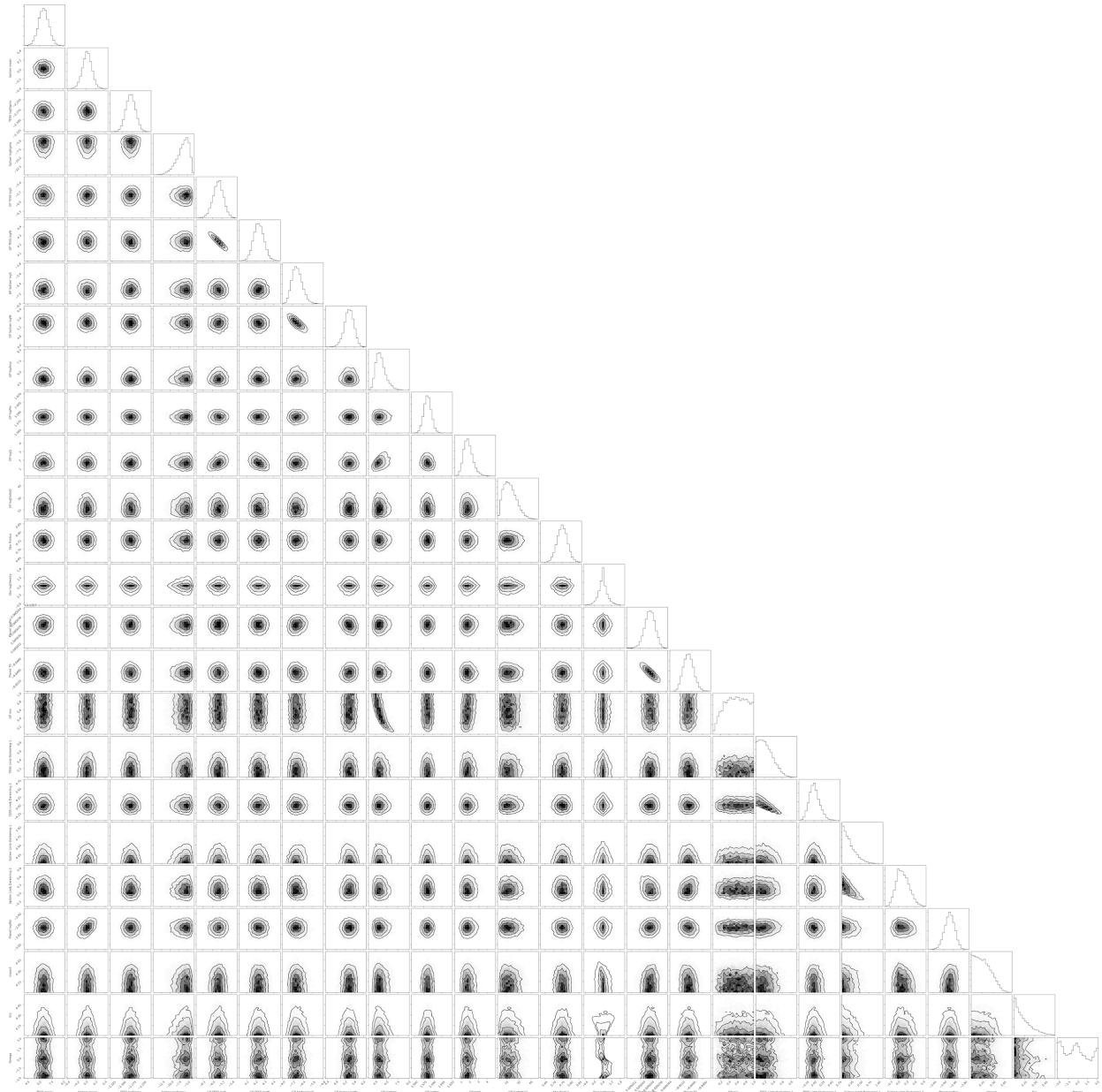
Extended Data Figure 2 MCMC corner plot for custom combined Spitzer and TESS light curve analysis for AU Mic. The full set of model parameters are shown, with the posterior probability distributions along the diagonal and covariance plots between parameters off-axis.

Ground-based light curve analysis

Ref 21 conducted a dedicated ground-based search for planets transiting AU Mic. One candidate partial transit event ingress was observed (BJD=2453590.885), with a depth (flux dimming of the star) of ~3%. By itself, this could be attributed to a number of phenomena associated with the star's youth, debris disk, or systematic errors. The photometric precision of this data is not sufficient to identify additional transits of AU Mic b or the candidate transit signal from the *TESS* light curve.

The SuperWASP team monitored AU Mic for seven seasons as part of a larger all-sky survey[22]. We visually inspect the SuperWASP light curve for evidence of any photometry consistent with an ingress or egress from a transiting planet. On several nights, given the ephemeris of AU Mic b, there are photometry visually similar to an ingress (for example, JD~2453978.40) or an egress (for example, JD~2454232.56). However, the amplitude of the brightness change is comparable to the amplitude of the red (low-frequency) noise in the SuperWASP light curve, and thus these features are likely not real. We do not model nor confirm these candidate events, given the stellar activity and relative photometric precision.

The ground-based photometric monitoring[21-22] of AU Mic establishes the long spot lifetimes, persisting for longer than a single observing season as evidenced by the lack of changes in the light curve over many stellar rotations, a defining characteristic of BY Dra variables. By comparing the TESS, SuperWASP and Ref 21 light curves, it is clear there is spot evolution on the time-scale of a few years, as the shape of the phased light curve does differ between the data sets.
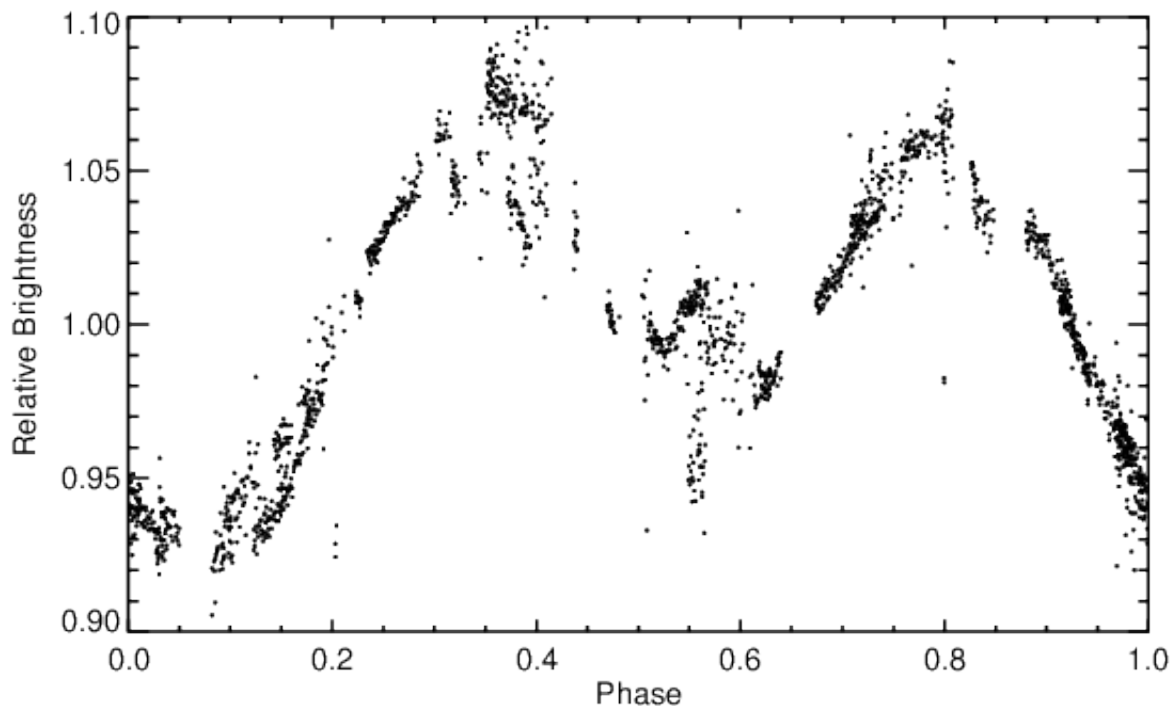

Extended Data Figure 3 One season (July-Oct 2007) of SuperWASP light curve for AU Mic, from the NASA Exoplanet Archive, phase-folded to to the rotation period of the star. Measurements with large photometric uncertainties (>5%) have been excluded from the plot. 1-σ measurement uncertainties are suppressed for visual clarity and are typically <1% but occasionally up to 5% at phases where there is more apparent vertical scatter in the measurement values themselves.

Radial Velocity Analysis

Seven RV data sets of AU Mic are obtained by our team or from the literature and archival data, and a detailed analysis to search for additional planets in the AU Mic system is a subject for future work. In this section, we present the utilization of the higher precision radial velocities from iSHELL, HARPS and HIRES to rule out higher mass companions, correlations with stellar activity, and confirm the planetary nature of AU Mic b by placing an upper limit on its mass. iSHELL[30] is a near-infrared echelle spectrometer with resolution of R=70,000 and simultaneous grasp of 300 nm at the 3.0-meter NASA Infrared Telescope Facility (IRTF), and equipped with our custom-built methane isotopologue absorption gas cell for wavelength calibration and instrument characterization[31]. The iSHELL data reduction and RV extraction follows the prescription in Ref 31. We combine our data with archival observations from the visible wavelength HARPS at the ESO La Silla 3.6-meter telescope[32], and the visible wavelength HIRES on the 10-meter Keck telescope[33] obtained for the California Planet Survey. All HARPS spectra were extracted and calibrated with the standard ESO Data Reduction Software, and radial velocities were measured using a least-squares template matching technique[34].

AU Mic is very active relative to a main-sequence dwarf, and we find RV peak-to-peak variations in excess of 400 m/s in the visible due to the rotational modulation of stellar activity (rms=175 m/s for HIRES and 115 m/s for HARPS). With iSHELL, the RVs exhibit stellar activity with a smaller but still significant peak-to-peak amplitude of ~150m/s (rms = 59 m/s). Consequently, no individual RV data set possesses a statistically significant periodogram signal at the period of planet b. This renders the mass detection of a planet with a velocity semi-amplitude smaller than the activity amplitude challenging[35-38].
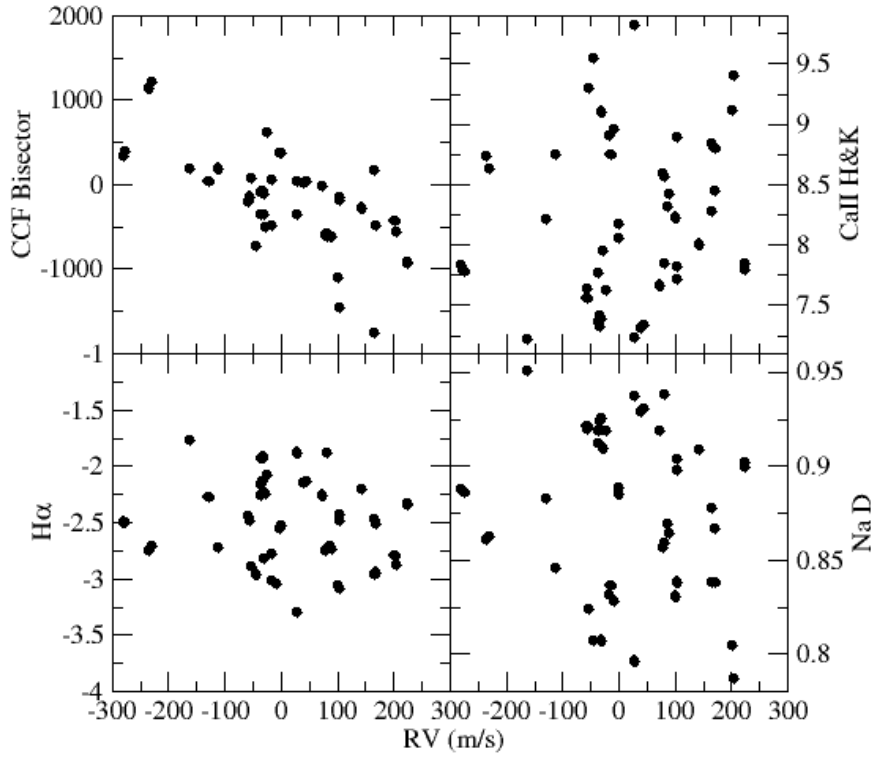
Extended Data Figure 4 Correlation plots of the standard HARPS stellar activity indicators with the RVs. The bisector values for the cross-correlation function, but not the activity indicators, show a correlation with the RVs, with significant remaining scatter. Formal uncertainties are smaller than the plotted symbols.
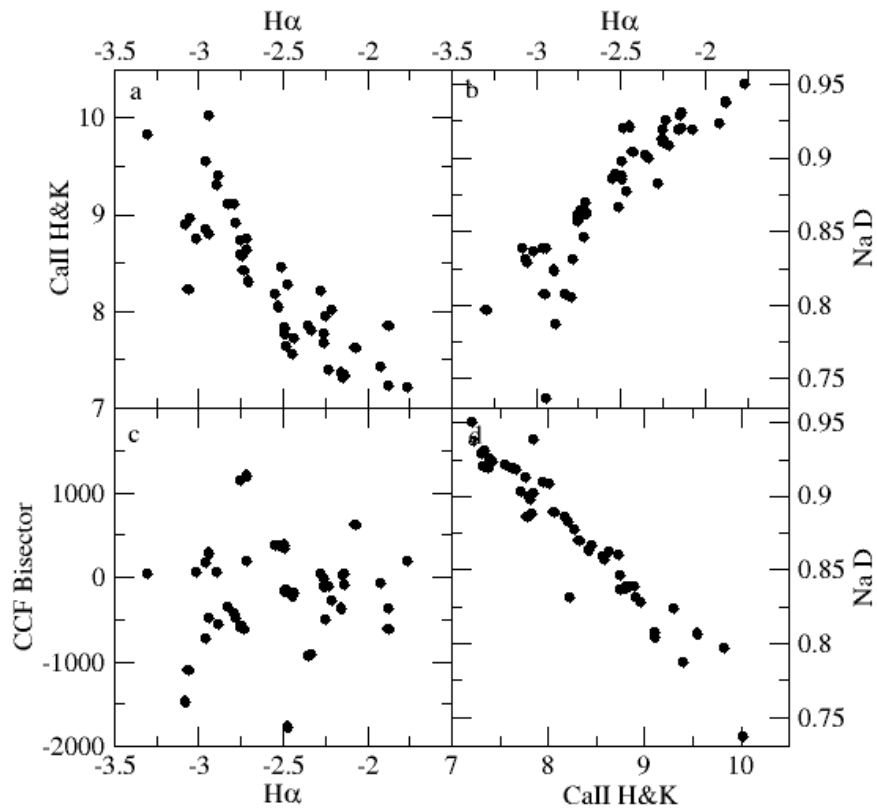
Extended Data Figure 5 Correlation plots of the HARPS activity indicators with each other. The activity indicators Calcium II H&K, Hα, and Sodium D activity indicators are strongly correlated with one another, but not with the RVs nor the CCF bisector.
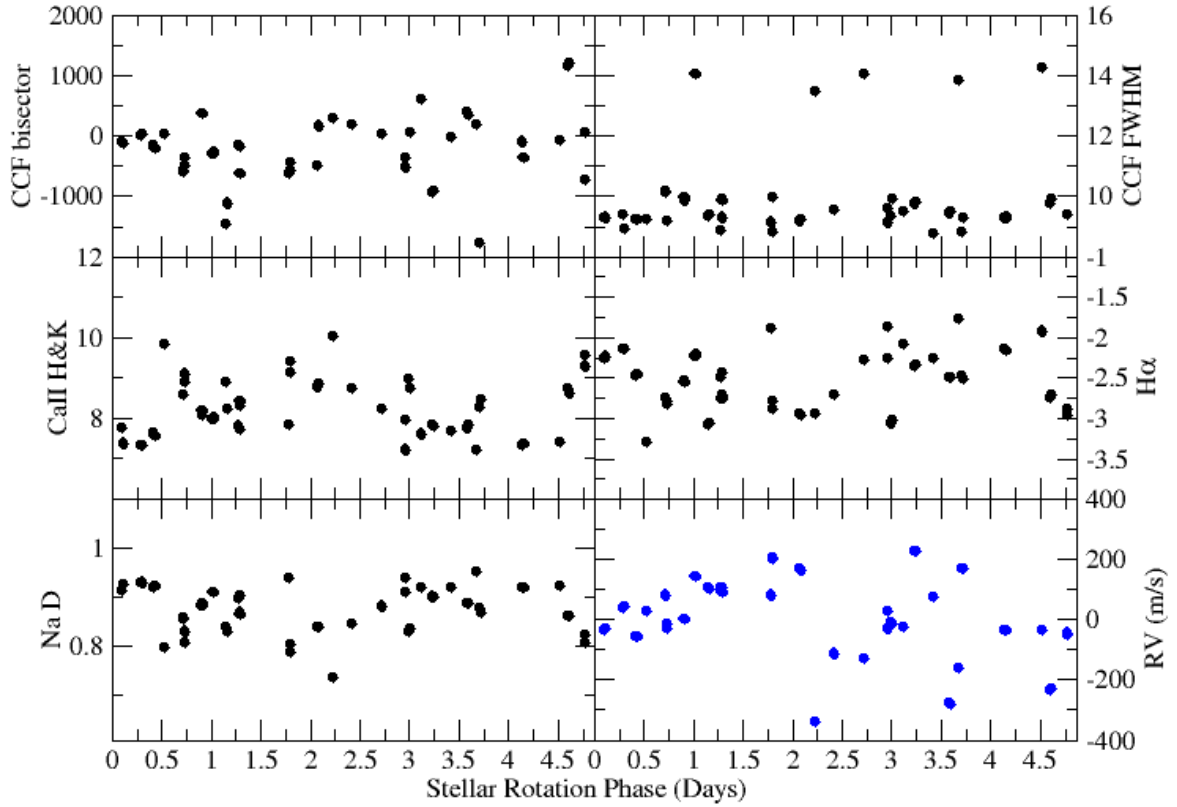
Extended Data Figure 6 The HARPS RVs (blue circles) and standard activity indicators (black circles), phase folded to the rotation period of the star. None of the activity indicators show a statistically significant trend with the period of AU Mic b. The Calcium and Sodium activity indicators do appear to show by eye some cyclic variation with the rotation period of the star, but it is not significant. Formal uncertainties are smaller than the plotted symbols.

We perform a MCMC simulation to model the stellar activity with a Gaussian Process (GP) simultaneously with a circular orbit model for AU Mic b using the regression tool RADVEL[39]. Offsets for each RV instruments velocity zero point are modeled. We fix the orbital period and time of transit conjunction (orbital phase) for AU Mic b to the best-fit values constrained by the TESS observations. We assume a velocity semi-amplitude prior with a width of 50% of the best-fit value and positive-definite. Due to the stellar activity and relatively sparse cadence sampling leading to GP model overfitting, no significant constraints on orbital eccentricity are possible; the eccentricity posterior distributions are unconstrained over the range of eccentricities allowed. Thus, for the sake of brevity we present herein only scenarios with fixed circular orbits, although eccentric orbits are considered. Constraining the eccentricities (and periastron angle) of AU Mic b will require a more intensive RV cadence and/or new modeling and mitigation of stellar activity beyond a GP model.

The stellar activity is modeled as a GP with a four "hyper-parameter" auto-correlation function that accounts for the activity amplitude, rotation period of the star modulating the starspots, and spot lifetimes treated as an autocorrelation decay[37,40]. From photometric time-series, the spot lifetime for AU Mic is observed to be longer than an observing season, a defining characteristic of BY Draconis-type variables such as AU Mic. Combined with its known rotation period, this enables us to generate priors on the Gaussian Process hyper-parameters. We use a Jeffrey's prior on the GP hyper-parameter activity amplitudes bounded between 1 and 400 m/s for the visible, and 1 and 200 m/s for the near-infrared, a spot decay lifetime prior that is a Gaussian centered on 110 days with a width of 25 days, a stellar rotation period prior of a Gaussian centered on 4.863 days with a width of 0.005 days, and a Gaussian prior centered on 0.388 with a width of 5% for the fourth hyper-parameter. We assess the dependence of our model comparison on the priors and prior widths used for the planet and GP parameters, which yield qualitatively similar results.
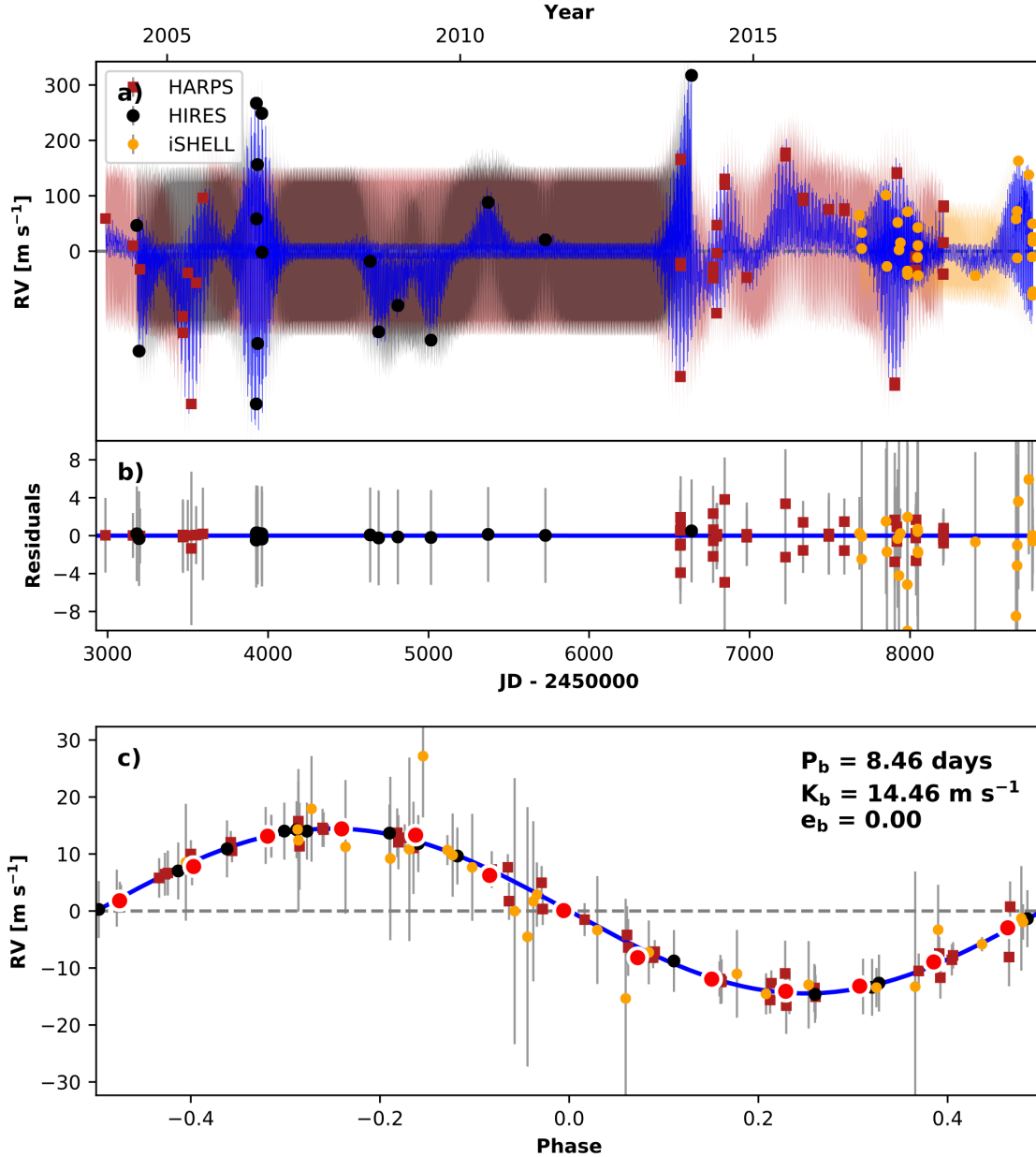
Extended Data Figure 7 a RV time-series of AU Mic with data from the iSHELL (yellow circles), High Resolution Spectrograph (HIRES, black circles) and High Accuracy Radial velocity Planet Searcher (HARPS, red squares) spectrometers. Uncertainties shown are 1-σ for HARPS and iSHELL. For HIRES, a 5 m/s minimum 1-σ uncertainty is adopted although the formal 1-σ uncertainties are smaller for all but one epoch at 5.43 m/s. The maximum-likelihood best fit model is overlaid in blue, with shaded regions indicating the 1-σ model confidence interval, with a separate GP for each data set indicated with different colored shaded regions. **b** Model-subtracted residuals, with the same colors as in a. Because our RVs are undersampled with respect to the stellar rotation period[38], the Gaussian Process best-fit model overfits the AU Mic RV time-series. **c** RV measurements are phased to the orbital period of AU Mic b, and binned in phase (red circles). The blue curve is a maximum-likelihood best-fit circular orbit model, after

subtracting the best fit GP model of stellar activity and the modeled instrument offsets. The plot is labeled with the best-fit orbital period and velocity semi-amplitude.
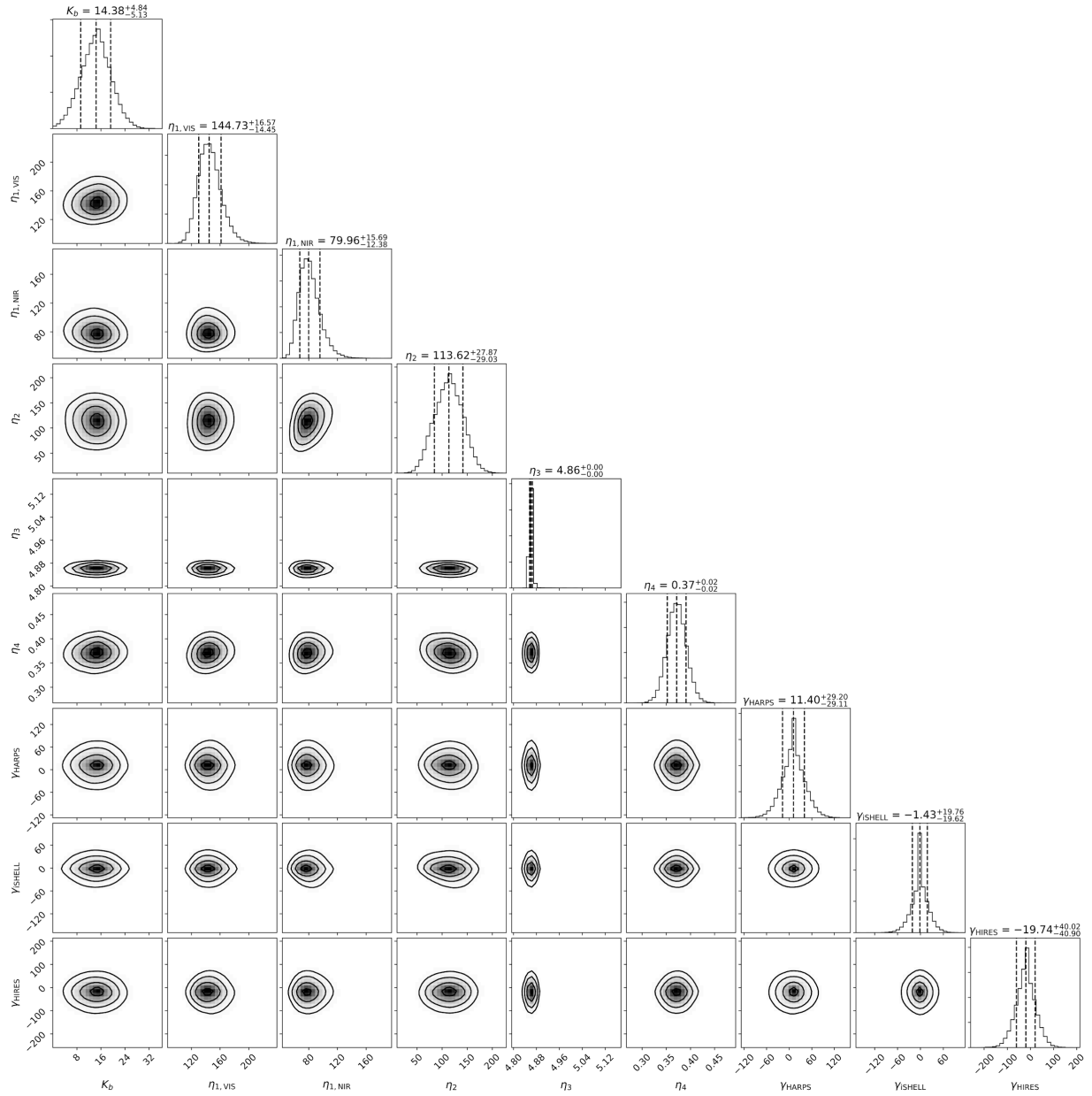
Extended Data Figure 8 RADVEL MCMC corner plot for the model parameters for the iSHELL, HARPS and HIRES RV data sets. Along the diagonal are the one-dimensional posterior probability distributions for a given model parameter; the others are the two-dimensional parameter covariance plots.

We use the MCMC simulations to compare statistically favored models from evaluating the model log-likelihoods, AICc and BIC statistics, and to provide robust characterization of model parameter uncertainties (e.g. posterior probability distributions). We derive an upper limit to the

velocity reflex motion from AU Mic b of of K<28.9 m/s at 3-σ confidence, corresponding to a mass upper limit of M_b<0.18 $M_{Jupiter}$ or <3.4 $M_{Neptune}$. We restrict our analysis to estimating an upper limit to the mass of AU Mic b for a number of reasons. First, while our statistical analysis favors the detection of AU Mic b, we do not rule out a non-detection at high statistical confidence. Second, our analysis also relies on the assumption that a GP model is an adequate model for stellar activity. Studies of other starspot-dominated convective M dwarfs[38] suggest this is adequate, but additional future observations and modeling efforts are needed, particularly for stars as active as AU Mic. From Kepler photometric time-series of main sequence stars, we demonstrated[40] that stellar activity should not introduce significant power in densely-sampled (~nightly) RV time-series at orbital periods longer than the stellar rotation period, as is the case for AU Mic b. However, for more sparsely sampled RV cadences such as ours, stellar activity can introduce apparent periodicities at time-scales longer than the stellar rotation period that can persist for several seasons[41]. The long-term magnetic activity evolution of AU Mic on timescales >100 days is also neither constrained nor modeled.

Extended Data Table 1. Model Comparison Results

AU Mic Model (all include GP & data set offsets)	RV data sets	Free Parameters	Number of RV epochs	Best-fit model rms	log-likelihood	BIC	AICc	ΔAICc	AICc qualitative comparison
b	iSHELL, HARPS, HIRES	9	91	2.68	-505.14	1050.88	1030.50	0	Favored Model
Gaussian Process only	iSHELL, HARPS, HIRES	8	91	3.02	-509.05	1054.18	1035.85	5.35	Strongly disfavored

<u>Wavelength Dependence of Stellar Activity</u>

At NIR wavelengths, the expected stellar activity amplitude depends on the effective temperature contrast of the starspots to the photosphere and the effects of Zeeman broadening[35,42]. If the spot temperature contrast is small (e.g. a few hundred Kelvin), then the RV (and photometric) amplitude due to the rotational modulation of starspots should scale as 1/λ to first order. This is the case for the Sun.[43] From the HARPS RV rms, one would expect a RV rms at 2.3 μm of ~50 m/s if the HARPS RV rms is entirely ascribable to stellar activity from cool starspots or plages. However, if the spot temperature contrast is large (e.g. >1000 Kelvin), one would expect only a marginal (~10%) reduction in RV stellar activity amplitude in the NIR. AU Mic lies close but slightly above the theoretical expectation for cool starspots with small rather than large spot temperature contrast - showing an RV rms of 59 m/s, a reduction of ~⅔ overall in rms. The modeled GP hyperparameters for the GP amplitudes show a reduction of ~½ from the visible to the NIR.

Ref 21 obtained multi-band photometry of AU Mic over the course of several rotation periods in their search for transiting exoplanets. This work demonstrates that AU Mic exhibits a decreased amplitude of photometric variability as a function of wavelength, again consistent with cool starspots with a relatively small temperature contrast. This is also consistent with multi-band photometry of young pre-main sequence stars and the Sun[44-45].
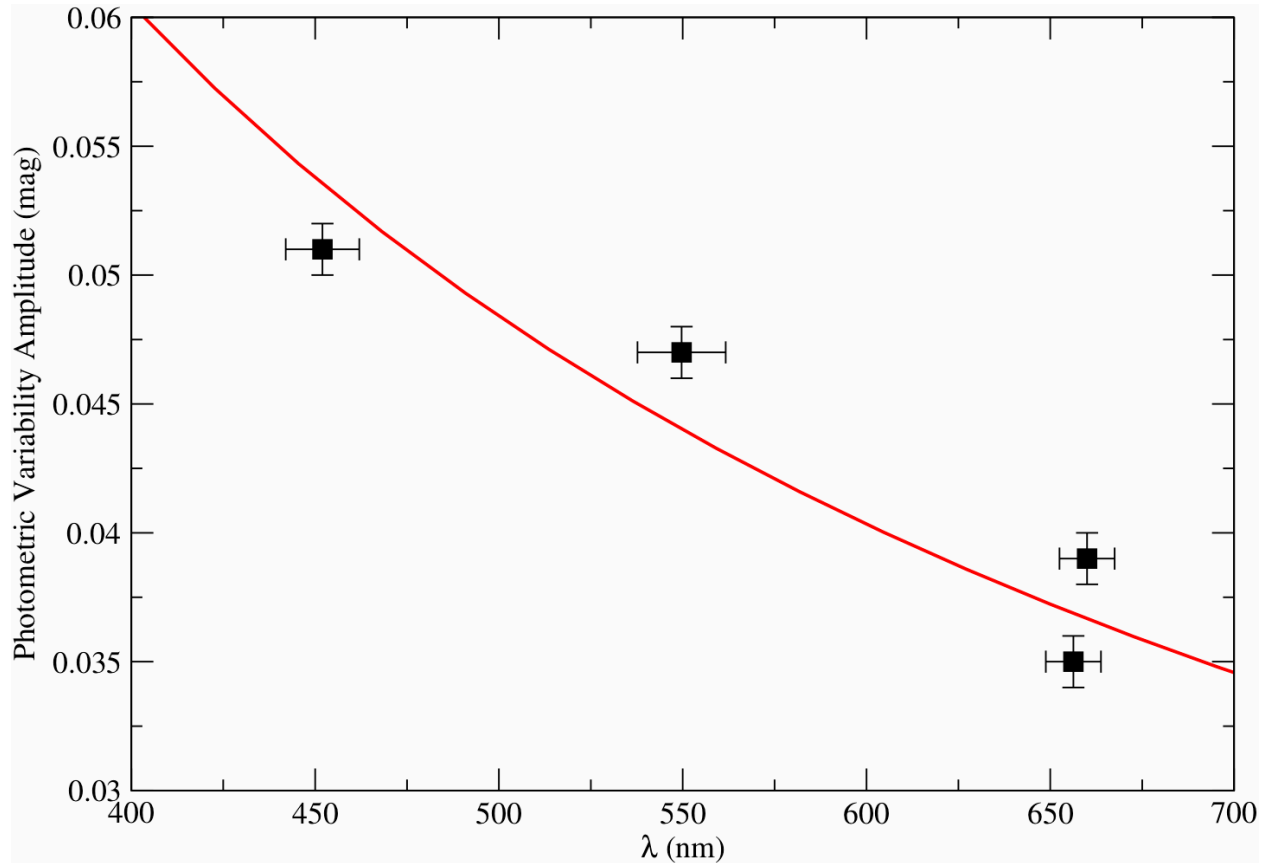
Extended Data Figure 9 Photometric variability amplitudes (black squares) observed by Ref 21 obtained contemporaneously in four different bandpasses. The horizontal error bars correspond to the effective bandpass widths and the 1-σ vertical error bars are set to 1 mmag. A 1/λ trend is shown in red, as would be expected for cool starspots with relatively small temperature contrast[35].

Host star parameters:

We compare the mass derived from the value from transit photometry plus CHARA radius to pre-main sequence solar-metallicity isochrones of Baraffe et al.[46] We logarithmically interpolate onto a finer grid, and fit to the absolute J,H, and K_s magnitudes (from 2MASS photometry and the Gaia parallax), the radius derived from CHARA[18] and the Gaia parallax, and the effective temperature. The best fit ($\chi2= 20.7, \nu=3$) age and mass are 19 Myr and 0.58 M_{Sun}; the uncertainties in age and mass are highly correlated, with a 95.4% confidence interval that spans 9-25 Myr, and 0.38-0.63 M_{Sun}.

Future work:

Additional RVs are necessary to increase the statistical confidence in the determination and recovery of the orbital parameters for AU Mic b and to search for additional planets. In particular, red-sensitive and NIR RVs with a nightly monitoring campaign for at least one season are necessary given the relatively large amplitude and time-scale of stellar activity, and if possible to search for additional Neptune-mass and smaller planets. Near-simultaneous chromatic RVs, taken at multiple wavelengths across the visible and NIR, and/or polarimetric observations may enable a future analysis that more robustly models the stellar activity than can be accomplished with GPs and the non-simultaneous multi-wavelength RVs presented herein. Simultaneous multi-wavelength RVs could isolate the chromatic stellar activity signal from the achromatic planet signals. Additionally, AU Mic has a v sin i of 8.7 km/s, Zeeman Doppler Imaging may enable a mapping of the spot configuration on the stellar surface of AU Mic to monitor long-term activity changes.

Future ground- and space-based photometric monitoring, particularly at red and infrared wavelengths, are needed to further constrain the transit parameters. Observing TTVs may be possible for this system to search for additional planets, but the analysis will be complicated by the rotational modulation of the starspots and flares. Flares occur frequently during transit, and since AU Mic b crosses active features on the stellar surface, this renders precise transit depth and duration measurements challenging. Here again, simultaneous multi-wavelength photometry could assist in distinguishing the transit signal from stellar activity. In particular, the Spitzer light curve presented herein and planned future observations will provide insights into the spot structure of the surface of AU Mic from spot-crossings by AU Mic b for cross-comparison to the Zeeman Doppler Imaging maps.

AU Mic b is also an interesting target to search for the signatures of its atmosphere, and the detection of extended hydrogen or helium exospheres, with multiple existing and planned near-term instrumentation on the ground and in space. Given its potentially low density, AU Mic b is one of the most favorable targets to search for planetary atmospheres, even taking into account the upper limit mass measurement. In particular, since the host star AU Mic is a young active star, it may promote the helium mass loss already detected in other Neptune-size bodies[47-48]. Thus, high-dispersion transmission spectroscopy with visible and near-infrared spectrographs, around the 1083 nm He I and the H alpha line, will measure or constrain atmospheric mass loss rate from this young warm planet.

Since the AU Mic system is young, nearby, possesses a debris disk and a planet that can be observed in transit, it provides an interesting laboratory to explore several theoretical issues. First, simulations should be carried out of the present and past interactions between the inner planet, the possible inner debris disk at <3 au[16], and outer debris disk including its clumpy structures[7,49-50]. These interactions depend on the masses of both the outer disk and the inner planet, so that this analysis could provide constraints on their properties; moreover, given the 22 Myr age of the star, these integrations can be carried out over the entire possible age of the

stellar system. Next, sensitive searches for trace gas could be carried out for this system. Until a few years ago, the classical definition of debris disk was the secondary generation of dust. Recently, an increasing number of debris do show gas (today up to 17 sources), including the debris disk orbiting Beta Pic[51], which is rich in carbon, oxygen and nitrogen, perhaps originating from icy grains rich in CO.

Finally, it would be useful to compare the properties of AU Mic b with predictions from planet formation/evolution models. If the mass of AU Mic b is close to our upper limit, the observed radius is close to its expected value for a several Gyr-old planet, whereas the predicted contraction time-scale of Neptune-size, gas-rich planets is longer than the age of the system[52-53]. These can be reconciled if the planet is significantly less massive than our upper limit. A better mass limit or determination could place interesting constraints on the entropy of planet formation and early thermal evolution.

<u>Code Availability</u>

All code that is not readily available on GitHub is available upon request.

<u>Data Availability</u>

In addition to the figure data available, all raw spectroscopic data is available either in the associated observatory archive or available upon request. The TESS light curve is available at the MAST archive, and the SuperWASP light curve is available at the NASA Exoplanet Archive.

Supplementary References:

20 Eggen, O.J.; "Narrow- and Broad-Band Photometry of Red Stars. II. Dwarfs." Astrophys. J. Supplement, 142, 16, 49 (1968).
21 Hebb, L; et al.; "A search for planets transiting the M-dwarf debris disc host, AU Microscopii." Mon. Not. R. Astron. Soc., 379, 1, 63-72 (2007).
22 Pollaco, D.L.; et al.; "The WASP Project and the SuperWASP Cameras." The Publications of the Astronomical Society of the Pacific, 118, 848, 1407-1418 (2006).
23 Jenkins, J.; et al.; "Overview of the Kepler Science Processing Pipeline." Astrophys. J.l Letters, 713, 2, L87-L91 (2010).
24 Jenkins, J.; et al.; "The TESS science processing operations center." Proceedings of the SPIE, 9913, 99133E (2016).
25 Eastman, Jason; Gaudi, B. Scott; Agol, Eric; "EXOFAST: A Fast Exoplanetary Fitting Suite in IDL." Publications of the Astronomical Society of the Pacific, 125, 923, 83 (2013).
26 Eastman, Jason; "EXOFASTv2: Generalized publication-quality exoplanet modeling code." Astrophysics Source Code Library, record ascl:1710.003
27 Kipping, D.; "Characterizing distant worlds with asterodensity profiling." Mon. Not. R. Astron. Soc., 440, 3, 2164-2184 (2014).

28 Stumpe, M.C.; et al.; "Multiscale Systematic Error Correction via Wavelet-Based Bandsplitting in Kepler Data." Proceedings of the Astronomical Society of the Pacific, 126, 100 (2014).

29 Smith, J.C.; et al.; "Kepler Presearch Data Conditioning II - A Bayesian Approach to Systematic Error Correction." Proceedings of the Astronomical Society of the Pacific, 124, 1000 (2012).

30 Rayner, J.T.; et al.; "iSHELL: a construction, assembly and testing." Proceedings of the SPIE, 9908, 990884 (2016)

31 Cale, B; et al."." Astronom. J., 158, 170 (2019)

32 Mayor, M.; et al.; "Setting new standards with HARPS." The Messenger 114, 20 (2003)

33 Howard, A.; et al.; "The California Planet Survey. I. Four New Giant Exoplanets." Astrophys. J., 721, 2, 1467-1481 (2010).

34 Anglada-Escudé, G. & Butler, R. P.; "The HARPS-TERRA Project. I. Description of the Algorithms, Performance, and New Measurements on a Few Remarkable Stars Observed by HARPS." Astrophys. J. Supplement, 200, 15 (2012).

35 Reiners, A.; Bean, J. L.; Huber, K. F.; Dreizler, S.; Seifahrt, A.; Czesla, S.; "Detecting Planets Around Very Low Mass Stars with the Radial Velocity Method." Astrophys. J., 710, 1, 432-443 (2010).

36 Tal-Or, L.; et al.; "The CARMENES search for exoplanets around M dwarfs. Radial-velocity variations of active stars in visual-channel spectra, " Astronomy & Astrophysics, 614, A122 (2018).

37 Haywood, R.; "Hide and Seek: Radial-Velocity Searches for Planets around Active Stars." PhD Thesis, University of St Andrews, (2015)

38 Barnes, J. R.; Jeffers, S. V.; Anglada-Escudé, G.; Haswell, C. A.; Jones, H. R. A.; Tuomi, M.; Feng, F.; Jenkins, J. S.; Petit, P.; "Recovering planet radial velocity signals in the presence of starspot activity in fully convective stars." Mon. Not. R. Astron. Soc., 466, 2, 1733-1740 (2017).

39 Fulton, Benjamin J.; Petigura, Erik A.; Blunt, Sarah; Sinukoff, Evan; "RadVel: The Radial Velocity Modeling Toolkit." Publications of the Astronomical Society of the Pacific, 130, 986, 044504 (2018)

40 Vanderburg, A.; et al.; "The Golidlocks Trap: Stellar Activity Masquerading as Habitable Exoplanets." Mon. Not. R. Astron. Soc., 459, 3565 (2016).

41 Nava, C; et al; "Exoplanet Imitators: A test of stellar activity behavior in radial velocity signals." eprint arXiv:1911.04106 (2019)

42 Reiners, A.; et al.; "Radial velocity signatures of Zeeman broadening." Astronomy & Astrophysics, 552, A103, (2013).

43 Marchwinski, R.C.; et al.; "Toward Understanding Stellar Radial Velocity Jitter as a Function of Wavelength: The Sun as a Proxy." The Astrophys. J., 798, 1, 63 (2015).

44 Cody, Ann-Marie; et al; "CSI 2264: Simultaneous Optical and Infrared Light Curves of Young Disk-bearing Stars in NGC 2264 with CoRoT and Spitzer—Evidence for Multiple Origins of Variability." Astron. J., 147, 4, 82 (2014).

45 Parks, J.R.; et al; "Periodic and Aperiodic Variability in the Molecular Cloud ρ Ophiuchus." Astrophys. J. Supplement, 211, 1, 3 (2014).

46 Baraffe, I.; et al.; "New evolutionary models for pre-main sequence and main sequence low-mass stars down to the hydrogen-burning limit." Astronomy & Astrophysics, 577, A42 (2015)

47 Nortmann, L.; et al. "Ground-based detection of an extended helium atmosphere in the Saturn-mass exoplanet WASP-69b." Science, 362, 6421, 1388-1391 (2018).

48 Allart, R.; et al.; "Spectrally resolved helium absorption from the extended atmosphere of a warm Neptune-mass exoplanet." Science, 362, 6421, 1384-1387 (2018).

49 Wang, J.; et al. "Gemini Planet Imager Observations of the AU Microscopii Debris Disk: Asymmetries within One Arcsecond." The Astrophysical Journal Letters, 811, 2, L19 (2015).

50 Roccatagliata, V.; et al.; "Long-wavelength observations of debris discs around sun-like stars." Astronomy & Astrophysics, 497, 2, 409-421 (2009).

51 Wilson, P. A.; Kerr, R.; Lecavelier des Etangs, A.; Bourrier, V.; Vidal-Madjar, A.; Kiefer, F.; Snellen, I. A. G.; "Detection of nitrogen gas in the β Pictoris circumstellar disc." Astronomy & Astrophysics, 621, A121 (2018).

52 Nettelmann, N.; et al; "Uranus evolution models with simple thermal boundary layers." Icarus, 275, 107. (2016)

53 Linder, E.; et al.; "Evolutionary models of cold and low-mass planets: cooling curves, magnitudes, and detectability." Astronomy & Astrophysics, 623, A85 (2019).

Author Information Reprints and permissions information is available at npg.nature.com/reprintsandpermissions. The authors declare no competing financial interests. Correspondence and requests for materials should be addressed to P.P.P. (pplavcha@gmu.edu).

PP - lead author, principal investigator for CSHELL/iSHELL gas cell and observations, analysis and interpretation; JG,PG,BC,AT,SXW RW - CSHELL/iSHELL data reduction & forward model codes; WM - RADVEL analysis; TB,DD,SQ,DFM,EG,CH,DK,EK,EQ,AV - analysis of TESS light curve; KS,KC,NN,EP,JP - follow-up ground-based observations; IJMC,DB,PL - Spitzer light curve; DF, BT,CH - inspection of ground-based light curves; DL - TRES; GA-E - HARPS; GR, RV,SS,JW,JJ - TESS mission architect; SR,AK,SD,JT - TESS mission; FA,MC,MK,AR,VR,JW - disk physics; DAA,JES,AY - flare analysis; CAB,MB,CB,DC,SRK,BM,SM,KvB - CSHELL/iSHELL instrumentation; BB,CB,JC,JH,JK,JO,CGT,RW,DJW,HZ - MINERVA-Australis; AC,CD,EF,CG,FG,RH,TH,JH,CK,MM,TM,AN,JT,BW,DW,PZ - CSHELL/iSHELL observer; EG - stellar parameters; AH - Keck HIRES.

ORCIDs:
Peter Plavchan - 0000-0002-8864-1667
Jonathan Gagné - 0000-0002-2592-9612
Peter Gao - 0000-0002-8518-9601
Bryson Cale - 0000-0001-6279-0595
William Matzko - 0000-0003-3937-562X
Sam Quinn - 0000-0002-8964-8377
Dax Feliz - 0000-0002-2457-7889
Keivan Stassun - 0000-0002-3481-9052
David W. Latham - 0000-0001-9911-7388
Tom Barclay - 0000-0001-7139-2724
Diana Dragomir - 0000-0003-2313-467X
Ben Tieu - 0000-0001-5773-7159
George Ricker - 0000-0003-2058-6662
Roland Vanderspek - 0000-0001-6763-6562
Sara Seager - 0000-0002-6892-6948
Joshua N. Winn - 0000-0002-4265-047X
Jon M. Jenkins - 0000-0002-4715-9460
Stephen Rinehart - none

Akshata Krishnamurthy - 0000-0002-8781-2743
Scott Dynes - 0000-0001-7010-0937
John Doty - 0000-0003-2996-8421
Fred Adams - 0000-0002-8167-1767
Dennis A Afanasev - 0000-0001-9526-9333
Guillem Anglada-Escudé - 0000-0002-3645-5977
Chas Beichman - 0000-0002-5627-5471
Mike Bottom - 0000-0003-1341-5531
Brendan Bowler - 0000-0003-2649-2288
Carolyn Brinkworth - 0000-0002-7897-4767
Carolyn J. Brown - 0000-0001-6649-4531
Andrew Cancino - none
David R. Ciardi - 0000-0002-5741-3047
Mark Clampin - none
Jake T. Clark 0000-0003-3964-4658
Karen Collins 0000-0001-6588-9574
Ian J.M. Crossfield - 0000-0002-1835-1891
Cassy Davison - 0000-0001-7392-9003
Daniel Foreman-Mackey - 0000-0002-9328-5652
Elise Furlan - 0000-0001-9800-6248
Eric Gaidos - 0000-0002-5258-6846
Claire Geneser - 0000-0001-9596-8820
Frank Giddens 0000-0003-2943-4729
Emily Gilbert - 0000-0002-0388-8004
Ryan Hall - none
Coel Hellier - 0000-0002-3439-1439
Todd Henry - 0000-0002-9061-2865
Jonathan Horner - 0000-0002-1160-7970
Andrew W. Howard - 0000-0001-8638-0320
Chelsea Huang - none
Joseph Huber - 0000-0002-1161-8274
Stephen R Kane - 0000-0002-7084-0529
Matthew Kenworthy - 0000-0002-7064-8270
John Kielkopf 0000-0003-0497-2651
David Kipping - 0000-0002-4365-7366
Chris Klenke - 0000-0002-9377-3007
Ethan Kruse - 0000-0002-0493-1342
Patrick Lowrance - 0000-0001-8014-0270
Bertrand Mennesson - 0000-0003-4205-4800
Matthew Mengel - 0000-0002-7830-6822
Sean M. Mills - 0000-0002-4535-6241
Tim Morton - none
Norio Narita - 0000-0001-8511-2981
America Nishimoto - none

Jack Okumura - 0000-0002-4876-8540
Enric Palle   0000-0003-0987-1593
Joshua Pepper 0000-0002-3827-8417
Elisa V. Quintana 0000-0003-1309-2904
Aki Roberge - 0000-0002-2989-3725
Veronica Roccatagliata - 0000-0002-4650-594X
Joshua E. Schlieder - 0000-0001-5347-7062
Angelle Tanner - 0000-0002-2903-2140
Johanna Teske - none
C. G. Tinney - 0000-0002-7595-0970
Andrew Vanderburg -0000-0001-7246-5438
Kaspar von Braun - 0000-0002-5823-4630
Bernie Walp - 0000-0001-6792-8637
Jason Wang - 0000-0003-0774-6502
Sharon Xuesong Wang - 0000-0002-6937-9034
Denise Weigand - 0000-0003-1095-568X
Russel White - 0000-0001-5313-7498
Rob Wittenmyer - 0000-0001-9957-9304
Duncan J. Wright - 0000-0001-7294-5386
Allison Youngblood - 0000-0002-1176-3391
Hui Zhang - 0000-0003-3491-6394
Perri Zilberman - 0000-0003-4714-0679